analytical chemistry

pubs.acs.org/ac Article

Bifunctional Pdots-Based Novel ECL Nanoprobe with Qualitative and Quantitative Dual Signal Amplification Characteristics for Trace Cytokine Analysis

Jinxia Liu,[†] Xiaodi Liu,[†] Huanhuan Chen, Luxia Yang, Aiting Cai, Haiwei Ji,* Qi Wang, Xiaobo Zhou, Guo Li, Mingmin Wu, Yuling Qin,* and Li Wu*

Cite This: *Anal. Chem.* 2022, 94, 7115−7122 Read Online

ACCESS | Metrics & More | Article Recommendations | Supporting Information

ABSTRACT: In this work, a novel methodology to design bifunctional ECL-luminophores with self-enhanced and TSA-amplified characteristics was proposed for improving the sensing performance of ECL-immunosensor toward trace cytokine analysis. Thanks to the qualitative- and quantitative- dual signal amplification technique, the as-prepared ECL biosensor demonstrated excellent detection performance. By analyzing the prospective cytokine biomarkers (IL-6), the ECL immunosensor exhibited a broad examination range with quite low detection limit and quite high selectivity, which was far superior to commercial ELISA kits and ever reported works. In particular, the novel ECL nanoprobe developed here could also be applied to monitor other immune toxicities or disease-related cytokines by using the respective antibodies corresponding to these targets. Moreover, the concept and construction strategy of self-amplified ECL-luminophores presented here could be further extended to design a series of Pdots-derived multicolored ECL probes to meet the needs of multipathway detection applications.

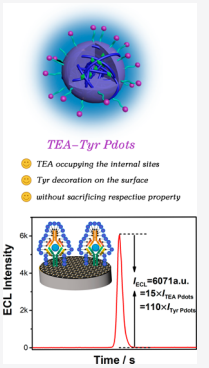

The emergence of immune checkpoint therapy (ICT) has subverted the configuration of conventional cancerous treatment and is deemed as the backbone of remedying certain malignancies.[1−3] The strategy of applying immune checkpoint inhibitors to take portions of the immune system brake off has realized tremendous success in yielding long-term responses, such as 10 years or more, in a significant subset of patients.[3−5] However, the following activated and potentiated immune reactions predispose patients to a high threat of immune-related adverse events (irAEs), happening in up to 80% of receiving ICT patients.[6,7] The high incident irAEs may arise during the therapy, offsetting the clinical strengths, leading to premature therapy cessation, further threatening the lives of certain patients.[8,9] To guarantee the successful execution of ICT, early identifying and vigilant monitoring irAEs by utilizing predictive biomarkers is imperative in avoiding harmful effects and matching therapeutic options.

Cytokines are potential to forecast the irAEs generation due to their outstanding characters in regulating the anticancer immune responses, consisting of increased antigen priming, up-modulating specific immune checkpoint molecules, and recruiting immune cells into tumor microenvironment.[7,10,11] Particularly in severe inflammation, excessive cytokine secretion has been widely considered as a major factor resulting in irAEs. The exertion of clinical cytokine analysis for irAE monitoring demands the technique that can detect cytokines with excellent selectivity and sensitivity,[7] particularly at the beginning of irAE progress (trace amount of cytokine). Conventional cytokine analyses, such as chemiluminescence immunoassay (CLIA) and enzyme-linked immunosorbent assay (ELISA) methods, allow scant capacity to detect low cytokine concentrations from blood in pg mL^{-1} level.[12,13] In addition, both ELISA and CLIA are limited by analysis time, detection channels, sample volume, and sensitivity, which makes it difficult for them to be developed as general approach to meet the various clinical cytokine analysis needs, especially for the measurement of trace targets.

Electrochemiluminescence (ECL) technique, integrating the merits of both electrochemical and photoluminescence analysis, shows strong detection performance in biomarkers analysis owing to its high sensitivity, wide dynamic range, low cost, and low-background signal interference, which is undoubtedly one of the best candidates for highly efficient irAEs assessment.[14] However, owing to the requirement of extra added coreactant and the short lifetime of coreactant radicals, the operations is tedious and the initial ECL efficiency is still unsatisfactory.[15] To address this issue, covalently conjugating the luminophore and the corresponding coreactant into the same system to prepare self-enhanced ECL nano-luminophores is regarded as an effective means to improve the

Received: March 5, 2022
Accepted: April 20, 2022
Published: May 2, 2022

https://doi.org/10.1021/acs.analchem.2c01041
Anal. Chem. 2022, 94, 7115−7122

Scheme 1. (A) Comparison of the Conventional ECL Luminophore and Bi-Functional Pdots; (B) The Fabrication Process of ECL Immunosensor.

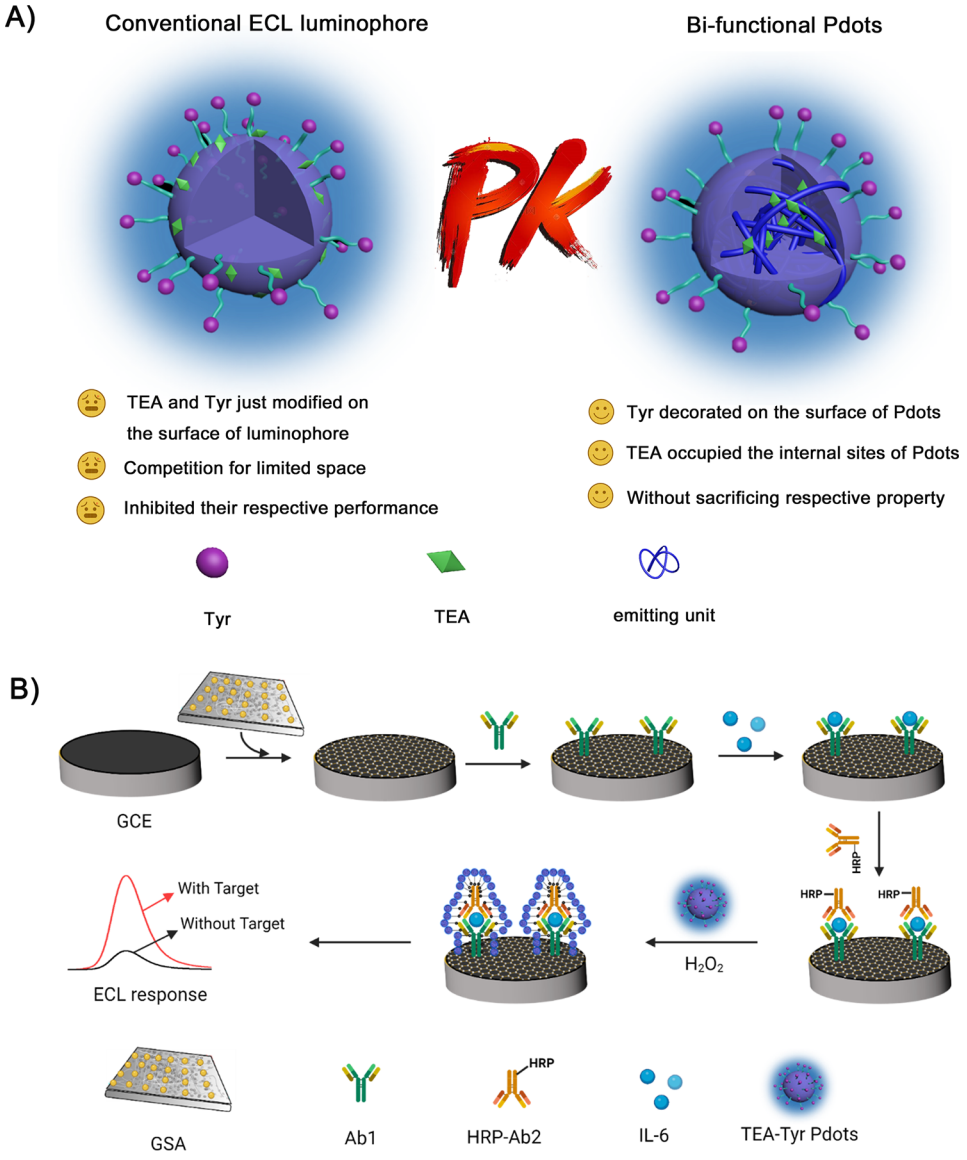

ECL efficiency.[16−18] Although promising, the method of improving individual signal probes' ECL-conversion efficiency, defined as qualitative amplification, still has a limited signal amplification capacity, which is difficult to meet many requirements for the analysis of trace biomarkers, especially in the clinical application scenarios. Converting a single biomolecular recognition event into as many output detectable signals as possible, defined as quantitative amplification, is another effective signal amplification strategy that is often used in biosensors construction.

As one of the typical representatives of the quantitative amplification strategy, tyramine signal amplification (TSA) technique has been widely applied in immunoassays by in situ increasing the number of signal tags per binding event and achieve enormous signal amplification.[19] In detail, the activated tyramine free-radical intermediate is in situ generated by HRP with the assistance of H_2O_2, then rapidly binding to amino acid residues of proteins. To achieve the goal of signal amplification with TSA method, tyramine (Tyr) unit is further introduced into signal reporters to build tags with specifically activated in situ signal amplification functions.[20,21] Inspired by the above successful cases, the TSA signal amplification concept can also be adopted in the construction of electrochemiluminescent probes, further enhancing the output ECL intensity from the quantitative dimension. However, to the best of our knowledge, there is no ECL emitters that can realize both the self-enhanced strategy based qualitative- and TSA based quantitative- dual signal amplification simultaneously has been reported so far, which may be limited by mutual interference from the technical level between the two approaches.

Herein, a bifunctional Pdots (TEA-Tyr Pdots) was designed to perfectly integrate self-enhanced ECL technology with TSA strategy and realized the quantitative- and qualitative- dual signal amplification in ECL biosensing for the first time. The main contributions of the as-developed smart ECL luminophore were summarized in Scheme 1A. As shown in Scheme 1A left, for conventional ECL-nanoluminophores, such as metal nanoclusters, quantum dots, etc., self-enhanced ECL or TSA strategy mainly achieved by introducing coreactants or

https://doi.org/10.1021/acs.analchem.2c01041
Anal. Chem. 2022, 94, 7115−7122

tyramine functional groups through covalent bonding on the surface of nanomaterials.[22,23] These two approaches would compete for limited space and binding sites, leading to the handicap to ensure their respective analytical performances simultaneously. The bifunctional Pdots designed here (Scheme 1A, right) could perfectly evade above shortcomings by giving full play to the structural advantages of Pdots itself, including diverse structures, designable functions, tunable emission colors, and high efficiency of photoelectric conversion.[24] On one hand, the coreactants (tertiary amine groups, TEA) occupying the internal bonding sites of Pdots were evenly and tightly distributed around the light-emitting units, thereby achieving efficient homogeneous electron transfer among the multiple light-emitting units and coreactions within the Pdots. On the other hand, tyramine group, fully occupying the external site on the surface of Pdots, could guarantee the efficiency of the enzyme-catalyzed TSA reaction thoroughly. Moreover, bifunctional Pdots-based ECL emitters could accommodate both coreactants and tyramine bifunctional groups properly without sacrificing their respective properties, further extremely exerting the signal amplification effect of the two parts. Ultimately, the well-designed Pdots were used as functional ECL probes to develop ECL sandwich-immunosensor for the sensitive and quantitative tests (Scheme 1B), in where interleukin 6 (IL-6) was measured as the example of target cytokine. Moreover, reduced graphene-mesoporous silica-gold hybrids (GSA) were employed as scaffold to control the spatial direction and position of the antibody precisely, further improving the biosensor's performance. The proposed immunosening platform for the determination of IL-6 could afford an ultrasensitive ECL response with quite low detection limit (ag mL^{-1} levels), which was below at least 6 orders of magnitude in contrast with the majority of reported methods and superior to commercial ELISA kit.

EXPERIMENTAL SECTION

Preparation of Tyramine-Coupled Amphiphilic Polymer (DSPE-PEG_{2000}-Tyr). The synthesis of amphiphilic polymer was shown in Supporting Information (SI) Scheme S1A. First, tyrosine (Fmoc-Tyr-OH) (20.2 mg, 0.05 mmol), DSPE-PEG_{2000}-NH_2 (100 mg, 0.05 mmol) and HBTU (56.9 mg, 0.15 mmol) were dissolved in DMF (10 mL) to form homogeneous solution. Then, DIEA (24.8 μL, 0.15 mmol) was dropwise added above mixture and stirred at room temperature (RT) for 3 h. Afterward, the solvent was removed by the lyophilizer, and then the crude product (DSPE-PEG_{2000}-Fmoc-Tyr) was obtained by centrifugation and washing with acetonitrile for 3 times. Then the crude product was added to 10 mL of 20% piperidine (THF: Piperidine = 4:1) and stirred for 30 min to remove the structure of Fmoc. The solvent was removed by filtering and drying in vacuum, and an appropriate amount of water was added to take the supernatant. The final product (DSPE-PEG_{2000}-Tyr) was obtained after freeze-drying and stored in a refrigerator at −20 °C.

Synthesis of Pdots. The Pdots was prepared by nanoprecipitation method with a little modification.[25] Briefly, conjugated polymer with tertiary groups (PFN-DOF) and amphiphilic polymer coupled with tyramine groups (DSPE-PEG_{2000}-Tyr) were respectively dissolved in THF to obtain stock solution (5 mg mL^{-1}). Subsequently, 60 μL of PFN-DOF and 40 μL of DSPE-PEG_{2000}-Tyr were mixed and then diluted with 300 μL of THF. The solution mixture was sonication for 1 min to form a homogeneous.

Next, the mixture was quickly injected into 2 mL of Milli-Q water under vigorous sonication in ice bath for 1 min. The THF solvent was removed by purging with nitrogen. Finally, the resulting dispersions were filtered through a 0.22 μm cellulose acetate membrane filter to obtain tertiary and tyramine bifunctionalized Pdots (TEA-Tyr Pdots) stock aqueous solution. Other two types Pdots were also prepared including tertiary embedded Pdots (TEA Pdots) by conjugated polymer with tertiary groups (PFN-DOF) and amphiphilic polymer coupled without tyramine groups (DSPE-PEG_{2000}-NH_2), as well as tyramine functionalized Pdots (Tyr Pdots) by conjugated polymer without tertiary groups (PFO) and amphiphilic polymer coupled with tyramine groups (DSPE-PEG_{2000}-Tyr). And the preparation route of three types of Pdots were shown in SI Scheme S1B.

Fabrication of ECL Immunosensor. The bare GCE was polished with Al_2O_3 powders such that it obtained a smooth mirror surface level. Then, GSA solution was dropped onto the electrode surface. After drying, 6 μL Ab1 solution (60 μg mL^{-1}) was modified onto the GSA/GCE interface and conducted at 37 °C for 1 h. Then, above-electrodes were covered with 6 μL of various concentrations of IL-6 and incubated at 37 °C for 1 h. In the following step, 6 μL Ab2-HRP solution (20 μg mL^{-1}) was dropped on the above-modified electrodes and incubated for 1 h. Furthermore, the mixture of TEA-Tyr Pdots and H_2O_2 (2.5 mM) was further incubated for 10 min to introduce the signal probes into the surface of proteins of the target IL-6 by TSA. The modified GCE was rinsed gently with PBS after each step reaction. In the end, the ECL detection was performed in 4 mL PBS (pH 7.4).

RESULTS AND DISCUSSION

Synthesis and Characterization of the Reduced Graphene-Mesoporous Silica Gold Hybrids (GSA). Generally, a sequential condensation reaction of amino-carboxyl group,[26] the cross-linking reaction of amino-glutaraldehyde (GA)-amino group,[27] or the interactions of Au NPs-amino group[28] is often employed to fix the antibody onto the electrode surface. However, the strategy can hardly regulate the spatial direction and position of the antibody on solid matrix precisely, bringing in the low detection reproducibility. Moreover, for sandwich-immunosensing establishment, low-density primary antibody (Ab1) immobilization is the novel path for promoting efficient antigen−antibody binding event to provide higher sensitivity and specificity. Based on this consideration, GSA was chosen in this work as the antibody loading platform for their dual function of both the control of antibody modifications and the prevention of nonspecific biomolecular adsorptions.[29,30] The detailed preparation and characterization of GSA was shown in SI Scheme S2 and Figures S1−S7. These results evidenced that GSA could be served as promising substrate for the construction of biosensor, not only improving the sensitivity of electrochemical response but also ensuring the stability of the biosensor. Here, the graphene-based nanocomposites possessed several merits: (a) the mesoporous silica structure was beneficial to decrease the nonspecific absorption between Au NPs and low-density biomolecules, which would help to reduce steric hindrance and improve the immune-binding efficiency. (b) The utilization of GSA can enlarge the electrode surface area and expose more

https://doi.org/10.1021/acs.analchem.2c01041
Anal. Chem. 2022, 94, 7115−7122

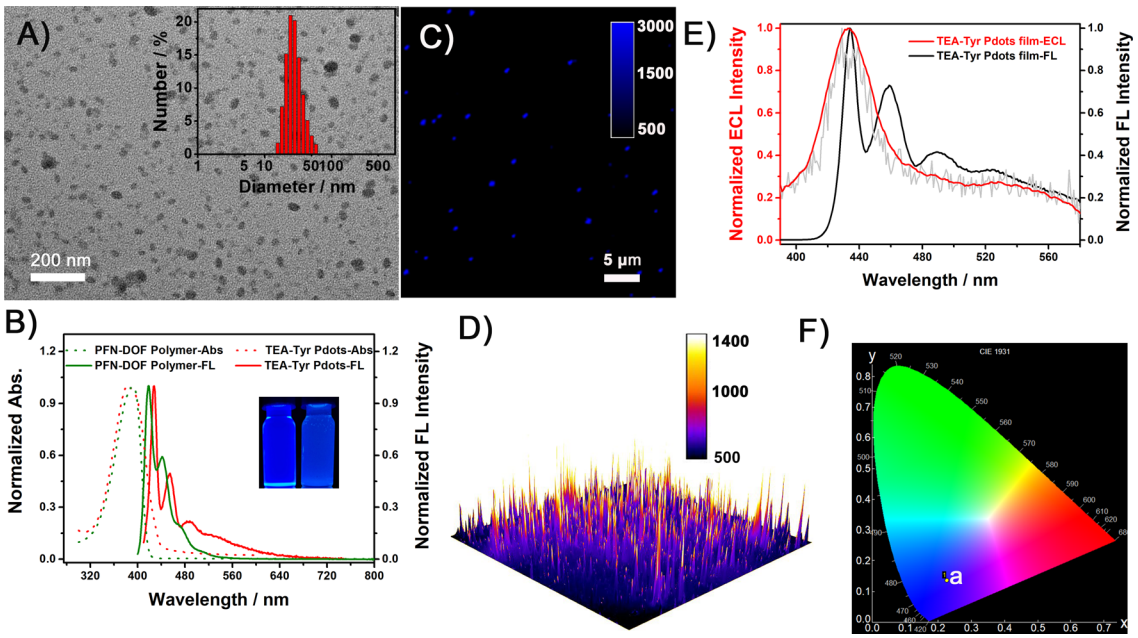

Figure 1. (A) TEM image of TEA-Tyr Pdots (the inset image shows the hydrodynamic diameter of TEA-Tyr Pdots measured by DLS). (B) Normalized UV−vis absorption and fluorescence spectrum of PFN-DOF polymer dilute in THF and TEA-Tyr Pdots dilute solution in water (the inset image shows the photographs of PFN-DOF polymer in THF (left) and TEA-Tyr Pdots in water (right) taken under 365 nm UV lamp). (C) Single-particle fluorescence images of TEA-Tyr Pdots. (D) 3D surface diagram of fluorescence images from (C). (E) Normalized fluorescence spectrum (black line) and ECL spectra (red line) of TEA-Tyr Pdots film. (F) CIE color diagram for the ECL emission of TEA-Tyr Pdots.

active sites to optimize the detective sensitivity. (c) The excellent conductivity of synergistic effect between reduced-graphene nanocomposite and Au NPs could further promote electron transfer and sensitivity.

Characterization of TEA-Tyr Pdots. The TEA-Tyr Pdots was prepared with nanoprecipitation method by blending conjugated polymer with tertiary groups (PFN-DOF) and amphiphilic polymer coupled with tyramine groups (DSPE-PEG_{2000}-Tyr). The characterizations of the functional amphiphilic polymer used in this work were given in SI Figure S8. The morphology and distribution of the obtained TEA-Tyr Pdots was characterized by TEM. As shown in Figure 1A, the TEA-Tyr Pdots displayed the excellent dispersion and spherical shape with a diameter around 20 nm, which was consistent with the dynamic light scattering (DLS) results of 25 nm (the inset of Figure 1A). And the hydration particle size of TEA Pdots and Tyr Pdots was about 25.5 nm (SI Figure S9A,B), which was close to the diameter of TEA-Tyr Pdots. The UV−vis absorption spectrum of the PFN-DOF polymer in THF and TEA-Tyr Pdots in water exhibited the similar distinct absorption peaks centered at 390 nm (Figure 1B), which could be ascribed to $\pi-\pi^*$ transition from the whole conjugated backbone.[31] It was obvious that fluorescence of PFN-DOF polymer in THF exhibited a characteristic well-resolved vibronic structure with peaks centered at 425, 450 nm and a shoulder around 480 nm (Figure 1B), respectively, which was due to the isolated polymer.[31] In contrast with PFN-DOF polymer, the fluorescence spectrum of TEA-Tyr Pdots showed an obvious red-shift by 10 nm owing to the increasing interchain interaction of the chain collapse.[32] Under 365 nm UV lamp irradiation, both PFN-DOF polymer in THF and TEA-Tyr Pdots in aqueous solution showed blue emission (inset in Figure 1B). In addition, the UV−vis absorption spectrum and fluorescence spectrum of the TEA Pdots and Tyr Pdots in H_2O was consistent with TEA-Tyr Pdots (SI Figure S9C,D), which was almost obvious change.

Meanwhile, the TEA-Tyr Pdots were apparently observed at the single-particle level of fluorescence brightness (Figure 1C), which were measured by fluorescence microscopy (405 nm laser excitation). Accordingly, 3D surface diagram of fluorescence images (Figure 1D) from Figure 1C demonstrated that the brightness of most single-particle was around 1400 counts. Furthermore, as shown in SI Figure S10, the relative FL quantum yield comparing to coumarin (CM) was 16%. The ECL spectrum of TEA-Tyr Pdots modified ITO occurred an emission peak at approximately 433 nm with corresponding potential of 1.6 V, which was consistent with the fluorescence emission peak of TEA-Tyr Pdots film at 435 nm (Figure 1E). This phenomenon demonstrated that ECL was generated from the band gap process of TEA-Tyr Pdots.[33] As shown in Figure 1F, the ECL of TEA-Tyr Pdots exhibited blue emission.

Electrochemical Characterizations and Electrochemiluminescence Measurements. In this system, a highly efficient TEA-Tyr Pdots based anodic ECL system was designed and constructed for further bioanalytical application. Tertiary amino groups was applied as the interior structure unit of Pdots, which acted as powerful "oxidative-reductive" coreactant for ECL generation in aqueous solution. Representative traces and proposed ECL mechanisms were summarized into four key steps (Figure 2A,B): (1) electrode oxidation, (2) deprotonation, (3) intramolecular electron transfer, (4) ECL emission. Specifically, both Tyr Pdots and TEA were electro-oxidized on the GCE at a similar positive scan. Like the widely used $Ru(bpy)_3^{2+}$-TPrA coreactant system,[34] the tertiary amines groups served as strong reductant after deprotonation, which could help to reduce the oxidized Tyr Pdots. Accordingly, strong ECL could be generated repeatedly by electrode oxidation. From Figure 2C, TEA-Tyr

https://doi.org/10.1021/acs.analchem.2c01041
Anal. Chem. 2022, 94, 7115−7122

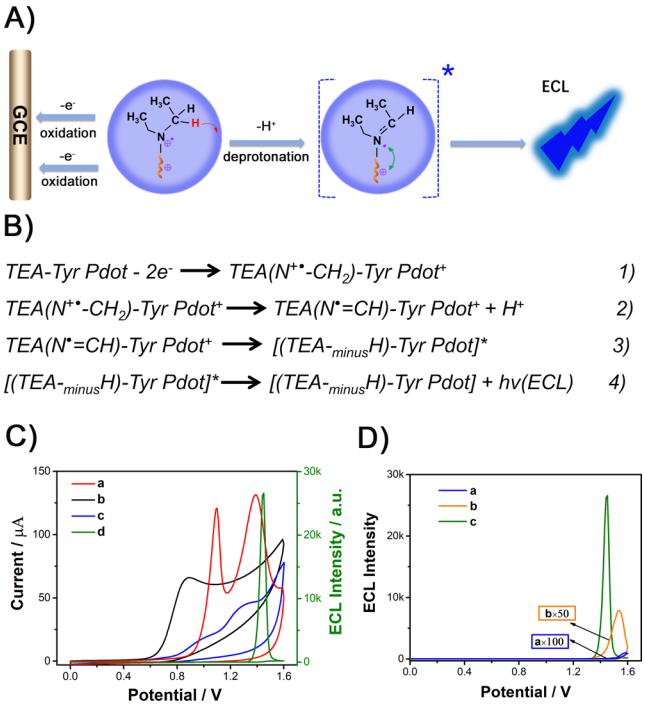

Figure 2. (A) ECL mechanism of TEA-Tyr Pdots. (B) Proposed pathways for ECL mechanism of TEA-Tyr Pdots. (C) CV curves of TEA-Tyr Pdots modified GCE (curve a), bare GCE in PBS containing 25 mM TEA (curve b), Tyr Pdots modified GCE (curve c) and ECL curve of TEA-Tyr Pdots modified GCE in 0.1 M PBS (curve d). (D) ECL curves of Tyr Pdots modified GCE measured in 0.1 M PBS (curve a), Tyr Pdots modified GCE tested in 0.1 M PBS containing 5 mM TEA (curve b), TEA-Tyr Pdots modified GCE scanned in 0.1 M PBS (curve c). Scan rate: 100 mV s^{-1} and potential versus Ag/AgCl.

Pdots modified electrode exhibited two oxidation peaks at 1.1 and 1.38 V (curve a). The first one was very close to the TEA oxidation peak with the similar onset potential at 0.88 V (curve b), implying the generation of cationic radicals ($TEA^{\bullet+}$-Tyr Pdots); the second one was consistent with the oxidation peak of Tyr Pdots (luminophores units) at 1.3 V (curve c). The ECL emission of TEA-Tyr Pdots could be obtained with the onset potential of 1.3 V (curve d) along with the oxidation of TEA and Tyr Pdots, demonstrating that the ECL emerging was largely determined by electron-oxidation of tertiary amine and Tyr Pdots.

To make a thorough inquiry with the emission mechanism, the ECL behavior in the absence of coreactants was recorded. As shown in Figure 2D, a relative lower intensity of ECL emission was observed for Tyr Pdots modified electrode (curve a), indicating the critical roles of coreactant TEA in the production of ECL. Furthermore, following the conventional coreactant route, when the Tyr Pdots/GCE was scanned in the bulk solutions with excess TEA (5 mM as coreactants in the 0.1 M PBS), the intensity of ECL emission remained low (Figure 2D, curve b). By contrast, a super high anodic ECL intensity was observed from TEA-Tyr Pdots (curve c) with the onset potential of +1.3 V and the peak potential located at +1.44 V, which was 168 times than Tyr Pdots in 5 mM TEA. The excellent ECL performance of TEA-Tyr Pdots attributed to the fact that grafted TEA closely dispersed around the luminescence body and worked as the coreactant to enhance the ECL performance of Tyr Pdots. Specifically, the highly efficient intramolecular electron transfer was a key factor owing to the shortened electron-transport distance and the enhanced efficiency of radical intermediates transport based-ECL process.[18] In addition, the ECL intensity of TEA Pdots/GCE in 0.1 M PBS was also measured to investigate whether tyramine group influence the ECL property of Pdots. As shown in SI Figure S11, the onset emission potential, peak potential and peak ECL intensity of TEA Pdots/GCE were identical with TEA-Tyr Pdots/GCE, indicating tyramine group almost no affecting the ECL performance of Pdots.

Mechanism of Signal Amplification. To emphasize the superiority of self-ECL and TSA strategy toward the IL-6 analysis, the contrast experiments had been performed to compare ECL signals from different probes. Specifically, Ab2-HRP/IL-6/Ab1/GSA/GCE electrode was incubated with the three signal probes in 2.5 mM H_2O_2 containing Tyr Pdots, TEA-Pdots, and TEA-Tyr Pdots. As can be seen in Figure 3A, there was no obvious ECL signal from the modified GCE under the Tyr Pdots incubation, which was ascribed to the lack of ECL coreactant. After the modified GCE incubated with TEA Pdots, a low ECL signal around 414 a.u. was observed owing to the nonspecific absorption of TEA Pdots (Figure 3B). Amazingly, ECL signal as high as ~6071 a.u. was achieved successfully if the modified GCE was incubated with TEA-Tyr Pdots probe (Figure 3C), which was 15 times the intensity of

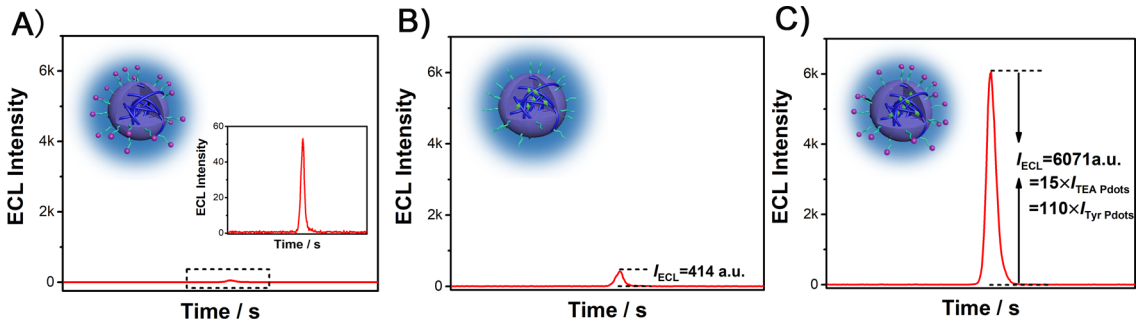

Figure 3. Feasibility of the immunosensor toward IL-6 analysis: ECL-time curves of (A) Tyr Pdots/Ab2-HRP/IL-6/Ab1/GSA/GCE, (B) TEA Pdots/Ab2-HRP/IL-6/Ab1/GSA/GCE, and (C) TEA-Tyr Pdots/Ab2-HRP/IL-6/Ab1/GSA/GCE. The inset photograph: the modified electrode (Ab2-HRP/IL-6/Ab1/GSA/GCE) was reacted with Tyr Pdots (A), TEA Pdots (B), and TEA-Tyr Pdots (C). IL-6 concentration: 100 pg mL^{-1}. The prepared immunosensor were detected in 4 mL PBS through setting photomultiplier tube at 1080 V and applying potential between 0 and 1.6 V with a scan rate of 100 mV s^{-1}, potential versus Ag/AgCl.

https://doi.org/10.1021/acs.analchem.2c01041
Anal. Chem. 2022, 94, 7115−7122

TEA Pdots and 110 times the intensity of Tyr Pdots, which was ascribed to the self-ECL and TSA strategy.

Analytical Ability of the ECL Immunosensor Toward IL-6. Primarily, CV and EIS measurements were employed to verify each fabrication step of the as-prepared immunosensor (SI Figure S12). Then, the as-established ECL platform was further applied to quantitate various concentrations of IL-6 and evaluate the biosensing performance under optimal conditions (SI Figure S13). What's more, in order to ensure the reaction efficiency of TSA, the fluorescence and ECL response of TEA-Tyr Pdots in H_2O_2 solution were explored. As shown in SI Figure S14, the fluorescence and ECL performance of TEA-Tyr Pdots was almost no obvious influence with incubation with a range of concentrations H_2O_2 solution. As shown in Figure 4A, with the increased concentration of IL-6, the ECL

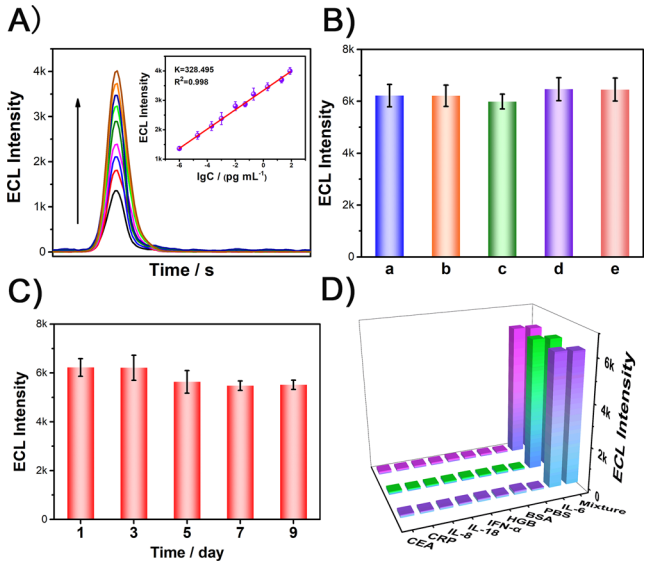

Figure 4. (A) ECL profiles of the proposed sensor with the incubation of different concentrations of IL-6 (from bottom to top): 20 ag mL^{-1}, 200 ag mL^{-1}, 1 fg mL^{-1}, 10 fg mL^{-1}, 50 fg mL^{-1}, 200 fg mL^{-1}, 2 pg mL^{-1}, 20 pg mL^{-1} and 80 pg mL^{-1} (inset: linear relationship between the ECL intensities and the logarithm of the concentrations of IL-6, the error bars represent the standard deviation of three repeated measurements). Reproducibility (a, b, c, d, and e represent five different immunosensors) (B) and stability (C) of the proposed immunosensor (IL-6:100 pg mL^{-1}, n = 3, error bar = SD). (D) Specificity of proposed ECL sensors with CEA (1 ng mL^{-1}), CRP (1 ng mL^{-1}), IL-8 (1 ng mL^{-1}), IL-18 (1 ng mL^{-1}), IFN-A (1 ng mL^{-1}), HGB (1 ng mL^{-1}), BSA (1 ng mL^{-1}), PBS, IL-6 (100 pg mL^{-1}), and mixture.

response of TEA-Tyr Pdots strengthened gradually since a large amount of TEA-Tyr Pdots was modified onto GCE based on tyramine signal amplification strategy. Correspondingly, the visualized linear equation was obtained between the logarithm of IL-6 concentration and ECL intensity, which was expressed by Y = 328.49 lgC + 3339.72, whose correlation coefficient was 0.998 (the inset of Figure 4A). The fabricated ECL biosensor exhibited a broad examination range from 20 ag mL^{-1} to 80 pg mL^{-1} accompanying a very low detection limit of 4 ag mL^{-1} (S/N = 3), which was superior to most of the previous reports (SI Table S1). Owing to the outstanding fluorescence characters of TEA-Tyr Pdots, TEA-Tyr Pdots was also employed as fluorescence probe to establish a fluorescence biosensor according to the construction strategy of sandwich-ECL immunosensing to detect IL-6. As shown in SI Figure S15A, the fluorescence intensity of TEA-Tyr Pdots gradually enhanced with the increased concentration of IL-6. The relevant linear curves were achieved between IL-6 concentration and fluorescence intensity (SI Figure S15B), and described as $I = 3.58 \times 10^4 \mathrm{lgC} + 1.41 \times 10^5$ (R^2 = 0.998). The linearity range of IL-6 ranged from 200 ag mL^{-1} to 100 fg mL^{-1} with the detection limit of 13 ag mL^{-1}. Although superior to commercial ELISA kit (SI Figure S16), the established fluorescence biosensor detection performance was still unmatched the ECL immunosensor fabricated in this work. Therefore, the splendid performance of the proposed ECL biosensor endued it huge potential for highly efficient detection of trace IL-6 in order to further fully meet the diagnostic requirement finally.

Reproducibility, Stability, and Selectivity of ECL Immunosensor. To evaluate the reliability of the immunosensor, reproducibility, stability, and selectivity performance were investigated. As a start, five immunosensors incubated with 100 pg mL^{-1} of IL-6 were recorded under identical conditions to estimate the reproducibility of the established ECL platform. The relative standard deviation (RSD) of the measurements was 3.4% (Figure 4B), illustrating the perfect reproducibility of the fabricated immunosensor. After that, stability of the developed sensor was also evaluated. As shown in Figure 4C, the immunosensors were stored under different periods and the ECL intensity still retained at least 89% of original intensity, demonstrating that the proposed immunosensor had satisfactory stability. In addition, selectivity was also a crucial index in the application of immunosensor. Several eventful interfering proteins (including CEA, CRP, IL-8, IL-18, IFN-α, HGB, and BSA) were applied to assess the selectivity of the state-of-art biosensor. As shown in Figure 4D, the ECL signal was inconspicuously observed from the protein interfering systems, which was similar to the blank signal (PBS). Whereas the detective signal from the mixture (100 pg mL^{-1} IL-6 + 1 ng mL^{-1} interferences) was almost the same as it from IL-6 system, which could be ascribed to the highly specific antigens/antibodies recognition and the effective coupling interfaces of GSA. Generally, it could be concluded that the as-prepared ECL biosensor exhibited satisfactory specificity, outstanding reproducibility and stability, which would further widen and deepen its diagnostic prospects.

Detection of Real Samples. The practical applicability of the proposed ECL sensor was explored to test IL-6 within human serum samples obtained from Affiliated Hospital of Nantong University and stored at 4 °C. Prior to the measurement, the serum samples were diluted 50-fold with PBS (pH 7.4). Then, the concentration was calculated by the linear equation of ECL response and multiplied by the dilution factor. The accuracy of the tested concentration of IL-6 in the serum samples was cross-examined with the ELISA Kit. As shown in SI Figure S16, the calibrated curve was described as Y = 0.00624 lgC + 0.08 (R^2 = 0.99). As comparison to ELISA kit, the detection of the as-prepared biosensor revealed the relative deviation of the two methods is less than 6.1% (SI Table S2). Moreover, the standard addition method was used to explore the ECL response of the exploited immunosensor in detecting IL-6 in human serum. As depicted in SI Table S3, the recovery rate range was between 95%−108%, and the corresponding RSD range was 1.2%−5.7%. These results indicated that the designed ECL immunosensor was promising in realistic clinical diagnosis.

https://doi.org/10.1021/acs.analchem.2c01041
Anal. Chem. 2022, 94, 7115−7122

CONCLUSIONS

In summary, a novel ECL immunosening platform was proposed based on bifunctional Pdots and reduced graphene-mesoporous silica gold hybrids for the ultrasensitive detection of IL-6. To be more specific, the Pdots with self-enhanced ECL and TSA amplified characteristics was first utilized as ECL luminophore to extremely amplify the signal from both qualitative- and quantitative- perspective. The coreactants (TEA) occupying the internal bonding sites of Pdots are evenly and tightly distributed around the light-emitting units, thereby achieving self-enhanced luminescence. Meanwhile, tyramine group (Tyr) distributed evenly on the surface of Pdots that could guarantee the efficiency of the enzyme-catalyzed TSA reaction thoroughly. The two synergistic effects improved the sensitivity of the immunosensor vastly. Additionally, as a scaffold, GSA regulated the antibody−antigen interactions on the electrode to reduce the no-specific absorption efficaciously. The proposed biosensor combined with a bifunctional Pdots and GSA provided promising strategy to realize efficient and sensitive ECL cytokine-analysis at quite low detection limit (ag mL^{-1} levels) for the first time, which is significant for early irAE (trace amount of cytokine) monitoring to further guarantee the successful execution of immune checkpoint therapy. Based on above-mentioned results, we also expect that the concept and construction strategy presented in this article could be extended to design a series of Pdots-derived multicolored ECL probes to meet the needs of multipathway detection.

ASSOCIATED CONTENT

Supporting Information

The Supporting Information is available free of charge at https://pubs.acs.org/doi/10.1021/acs.analchem.2c01041.

Materials and reagents; apparatus; synthesis route of the DSPE-PEG_{2000}-Tyr and preparation of Pdots, Scheme 1; synthesis and characterization of GSA, Scheme 2 and Figures S1−S7; characterization of DSPE-PEG_{2000}-Tyr, Figure S8; characterization of Pdots, Figures S9−S11; electrochemical characterizations of ECL immunosensor, Figure S12; optimization of the detection conditions, Figure S13; stability of TEA-Tyr Pdots in H_2O_2 solution, Figure S14; fluorescence detection of different concentrations of IL-6, Figure S15; ELISA kit detection of different concentrations of IL-6, Figure S16; comparison of different biosensors for IL-6 detection, Table S1; actual sample testing, Table S2; recovery tests, Table S3 (PDF)

AUTHOR INFORMATION

Corresponding Authors

Haiwei Ji − *School of Public Health, Nantong University, Nantong 226019, P. R. China*; Email: jihaiwei64@ntu.edu.cn

Yuling Qin − *School of Public Health, Nantong University, Nantong 226019, P. R. China*; Email: ylqin@ntu.edu.cn

Li Wu − *School of Public Health, Nantong University, Nantong 226019, P. R. China*; orcid.org/0000-0002-4118-7970; Email: wuli8686@ntu.edu.cn

Authors

Jinxia Liu − *School of Public Health, Nantong University, Nantong 226019, P. R. China*

Xiaodi Liu − *School of Public Health, Nantong University, Nantong 226019, P. R. China*

Huanhuan Chen − *School of Public Health, Nantong University, Nantong 226019, P. R. China*

Luxia Yang − *School of Public Health, Nantong University, Nantong 226019, P. R. China*

Aiting Cai − *School of Public Health, Nantong University, Nantong 226019, P. R. China*

Qi Wang − *School of Public Health, Nantong University, Nantong 226019, P. R. China*; orcid.org/0000-0001-5763-2357

Xiaobo Zhou − *School of Public Health, Nantong University, Nantong 226019, P. R. China*; orcid.org/0000-0001-9686-7968

Guo Li − *School of Public Health, Nantong University, Nantong 226019, P. R. China*

Mingmin Wu − *School of Public Health, Nantong University, Nantong 226019, P. R. China*

Complete contact information is available at: https://pubs.acs.org/10.1021/acs.analchem.2c01041

Author Contributions

†J.L. and X.L.contributed equally. This manuscript was written through the contributions of all authors. All authors have given approval to the final version of the manuscript.

Notes

The authors declare no competing financial interest.

ACKNOWLEDGMENTS

This work was supported by the National Natural Science Foundation of China (31901045, 32171452, 21877083, 31901056, 62005132, 62105165), Jiangsu Specially-Appointed Professor (06200048, 06200053), Jiangsu Innovative and Entrepreneurial Research Team Program, 2020 Nantong Science and Technology Plan Project (JC2020099, JC2020100), Large Instruments Open Foundation of Nantong University, and 2020 training program of innovation and entrepreneurship for college students of Nantong university.

REFERENCES

(1) Sharma, P.; Allison, J. P. *Cell* **2015**, *161*, 205−214.
(2) Sharma, P.; Allison, J. P. *Science* **2015**, *348*, 56−61.
(3) Sharma, P.; Allison, J. P. *Nat. Rev. Immunol.* **2020**, *20*, 75−76.
(4) Topalian, S. L.; Taube, J. M.; Anders, R. A.; Pardoll, D. M. *Nat. Rev. Cancer* **2016**, *16*, 275−287.
(5) Ribas, A.; Wolchok, J. D. *Science* **2018**, *359*, 1350−1355.
(6) Freeman-Keller, M.; Kim, Y.; Cronin, H.; Richards, A.; Gibney, G.; Weber, J. S. *Clin. Cancer Res.* **2016**, *22*, 886−894.
(7) Lim, S. Y.; Lee, J. H.; Gide, T. N.; Menzies, A. M.; Guminski, A.; Carlino, M. S.; Breen, E. J.; Yang, J. Y. H.; Ghazanfar, S.; Kefford, R. F.; Scolyer, R. A.; Long, G. V.; Rizos, H. *Clin. Cancer Res.* **2019**, *25*, 1557−1563.
(8) Yshii, L. M.; Hohlfeld, R.; Liblau, R. S. *Nat. Rev. Neurol.* **2017**, *13*, 755−763.
(9) Calabrese, L. H.; Calabrese, C.; Cappelli, L. C. *Nat. Rev. Rheumatol.* **2018**, *14*, 569−579.
(10) Johnson, D. B.; Balko, J. M. *Clin. Cancer Res.* **2019**, *25*, 1452−1454.
(11) Berraondo, P.; Sanmamed, M. F.; Ochoa, M. C.; Etxeberria, I.; Aznar, M. A.; Perez-Gracia, J. L.; Rodriguez-Ruiz, M. E.; Ponz-Sarvise, M.; Castanon, E.; Melero, I. *Br. J. Cancer* **2019**, *120*, 6−15.
(12) Hanash, S. M.; Pitteri, S. J.; Faca, V. M. *Nature* **2008**, *452*, 571−579.

(13) Malhotra, R.; Patel, V.; Vaqué, J. P.; Gutkind, J. S.; Rusling, J. F. *Anal. Chem.* **2010**, *82*, 3118−3123.
(14) Zhang, K.; Fan, Z.; Yao, B.; Zhang, T.; Ding, Y.; Zhu, S.; Xie, M. *Biosens. Bioelectron.* **2021**, *176*, 112942.
(15) Qi, H.; Zhang, C. *Anal. Chem.* **2020**, *92*, 524−534.
(16) Li, J. S.; Jia, H. Y.; Ren, X.; Li, Y. Y.; Liu, L.; Feng, R. Q.; Ma, H. M.; Wei, Q. *Small* **2022**, *18*, 202106567.
(17) Carrara, S.; Arcudi, F.; Prato, M.; De Cola, L. *Angew. Chem., Int. Ed.* **2017**, *56*, 4757−4761.
(18) Wang, T.; Wang, D.; Padelford, J. W.; Jiang, J.; Wang, G. *J. Am. Chem. Soc.* **2016**, *138*, 6380−6383.
(19) Akama, K.; Shirai, K.; Suzuki, S. *Anal. Chem.* **2016**, *88*, 7123−7129.
(20) Zhou, J.; Tang, J.; Chen, G.; Tang, D. *Biosens. Bioelectron.* **2014**, *54*, 323−328.
(21) Yuan, L.; Xu, L.; Liu, S. *Anal. Chem.* **2012**, *84*, 10737−10744.
(22) Chen, F.; Wang, D.; Chen, J.; Ling, J.; Yue, H.; Gou, L.; Tang, H. *Sensor Actuat. B-Chem.* **2020**, *305*, 127472.
(23) Han, T. T.; Dong, H.; Ren, L. L.; Bao, N.; Wu, W. Z.; Ding, S. N. *Chem. Commun.* **2017**, *53*, 5388−5391.
(24) Yu, J. B.; Rong, Y.; Kuo, C. T.; Zhou, X. H.; Chiu, D. T. *Anal. Chem.* **2017**, *89*, 42−56.
(25) Chen, H.; Yu, J.; Men, X.; Zhang, J.; Ding, Z.; Jiang, Y.; Wu, C.; Chiu, D. T. *Angew. Chem., Int. Ed.* **2021**, *133*, 12114−12119.
(26) Shen, J.; Li, Y.; Gu, H.; Xia, F.; Zuo, X. *Chem. Rev.* **2014**, *114*, 7631−7677.
(27) Wang, C.; Li, Z.; Ju, H. *Anal. Chem.* **2021**, *93*, 14878−14884.
(28) Ai, Z.; Zhao, M.; Han, D.; Chen, K.; Xiong, D.; Tang, H. *Biosens. Bioelectron.* **2021**, *179*, 113059.
(29) Lin, Y. H.; Wu, L.; Huang, Y. Y.; Ren, J. S.; Qu, X. G. *Chem. Sci.* **2015**, *6*, 1272−1276.
(30) Yang, S.; Feng, X.; Wang, L.; Tang, K.; Maier, J.; Müllen, K. *Angew. Chem., Int. Ed.* **2010**, *49*, 4795−4799.
(31) Ma, L.; Wu, N.; Liu, Y.; Ran, X.; Xiao, D. *Electrochim. Acta* **2019**, *297*, 826−832.
(32) Wu, C.; Bull, B.; Szymanski, C.; Christensen, K.; McNeill, J. *ACS Nano* **2008**, *2*, 2415−2423.
(33) Bae, Y.; Myung, N.; Bard, A. J. *Nano Lett.* **2004**, *4*, 1153−1161.
(34) Zhou, X.; Zhu, D.; Liao, Y.; Liu, W.; Liu, H.; Ma, Z.; Xing, D. *Nat. Protoc.* **2014**, *9*, 1146−1159.

https://doi.org/10.1021/acs.analchem.2c01041
Anal. Chem. 2022, 94, 7115−7122